

Recurrence due to periodic multi-soliton fission in the defocusing nonlinear Schrödinger equation

Guo Deng¹, Sitai Li², Gino Biondini^{1,2}, and Stefano Trillo³

¹*Department of Physics, State University of New York at Buffalo, Buffalo, New York 14260, USA*

²*Department of Mathematics, State University of New York at Buffalo, Buffalo, New York 14260, USA*

³*Department of Engineering, University of Ferrara, Via Saragat 1, 44122 Ferrara, Italy*

(Dated: November 19, 2021)

We address the degree of universality of the Fermi-Pasta-Ulam recurrence induced by multisoliton fission from a harmonic excitation by analysing the case of the semiclassical defocusing nonlinear Schrödinger equation, which models nonlinear wave propagation in a variety of physical settings. Using a suitable Wentzel-Kramers-Brillouin approach to the solution of the associated scattering problem we accurately predict, in full analytical way, the number and the features (amplitude and velocity) of soliton-like excitations emerging post-breaking, as a function of the dispersion smallness parameter. This also permits to predict and analyse the near-recurrences, thereby inferring the universal character of the mechanism originally discovered for the Korteweg-deVries equation. We show, however, that important differences exist between the two models, arising from the different scaling rules obeyed by the soliton velocities.

PACS numbers: 02.30.Ik, 05.45.Yv, 42.65.Sf, 47.20.-k

I. INTRODUCTION

The discovery by Fermi-Pasta-Ulam (FPU) that a low frequency excitation of nonlinear oscillator chains give rise to recurrence instead of equipartition, a phenomenon now known as FPU recurrence [1, 2], turned into one of most consequential findings of nonlinear physics [3–7], leading to multiple research avenues which are still actively investigated today [8–11]. The first resolution of the apparent paradox was given ten years later by Zabusky and Kruskal (ZK) [12] who showed that in the continuum limit that gives rise to the weakly dispersive Korteweg-de Vries (KdV) equation [13], the recurrence can be understood in terms of solitons, that fission from points of breaking (shocks) occurring in the periodic input mode (a regime which is substantially confirmed, e.g. for the quadratic, or so-called α -type, FPU chain [14]). Nearly synchronous arrival of the solitons after interaction leads to the recursion. An explicit estimate for the KdV recurrence time was then given by Toda [15, 16]. Experimentally, the recurrence from periodic input was reported in different systems ranging from electrical lattice networks [17] to continuous wave systems such as ion acoustic plasma waves [18], and gravity waves in shallow water [19], while it could be potentially observed also for electron beams that exhibit KdV type of breaking [20].

This result has led to the notion that a time scale exists for which the dynamics of FPU is essentially integrable, that is, it remains close to integrable limits, either the KdV in the continuum approximation or the discrete Toda chain [8, 21]. Over much longer times the FPU chains eventually thermalise, as it is now clear after decades of research on this topics [8, 9]. A crucially important remaining issue, however, is to investigate the metastable state characterised by the recurrences at intermediate time scales. In this context, a natural question that has remained surprisingly unaddressed is *the degree of universality of the mechanism discovered by ZK for other integrable models*. While it is now accepted that FPU recurrence is not

necessarily a prerogative of integrable models [11], the latter constitutes a wide and extremely important class employed to describe innumerable physical situations. Clearly, the importance of integrable systems goes well beyond the specific interest for FPU chains, since they often provide an accurate description of several genuinely continuous physical systems. In this context, breaking phenomena are a universal feature of the weakly dispersive regime [22] (see also [23] for a recent review) occurring for the nonlinear Schrödinger (NLS) equation [24–33], naturally arising as the continuum limit of cubic β -FPU [4], the Benjamin-Ono equation [34, 35] and the Toda lattice [36–38], to name only a few. A special role in this context is played by the *defocusing* or repulsive NLS equation, since it describes wave breaking phenomena recently observed and analysed in areas as different as nonlinear optics [26–32], Bose-Einstein condensates [24, 25], and spin waves [33]. Furthermore, the periodic input problem for such model was recently demonstrated to be accessible in fiber optics experiments, which show fission of dark “solitons” from periodic points of breaking [29, 30]. Yet, natural and fundamental questions concerning how to predict the number and the features of the solitons and whether recurrence should be expected remain to date completely open in such model.

The purpose of this paper is to give an answer to these questions and to demonstrate that soliton generation as a result of hydrodynamic-like instabilities, and the resulting FPU-like recurrences, are in fact a more general feature of nonlinear wave evolution equations with small dispersion. To this end, we show that such phenomena can be effectively treated analytically using the scattering problem and its finite gap formulation associated with the defocusing NLS equation. While our results significantly broaden the universality of the ZK mechanism of recurrence, they allow to clarify that the phenomenon presents, for the NLS equation, considerable differences with respect to the case of the KdV equation.

We remark that FPU recurrences have also been referred to in the literature in the focusing regime of the NLS equation.

These, however, are exact (instead of near) recurrences that occur through a different kind of mechanism involving modulation instability of a strong background (a forbidden regime for the defocusing NLS equation which is well known to be modulationally stable). Such scenarios have been investigated in fluids and optics only in a regime that involve few dominant Fourier modes, i.e. far from the weakly dispersive limit that we are interested in [39–44]. Conversely, wavepackets without background in the weakly dispersing limit of the focusing regime are known to exhibit a different type of breaking (i.e., elliptic umbilic catastrophe [45]) compared with the defocusing case. The complicated dynamics in the evolution stage beyond the catastrophe cannot be reduced, in general, to the fission of solitons that simply move apart with different velocities [46, 47]. Moreover the global scenario for a periodic input mode in the focusing regime was never addressed so far, and will require a specific analysis that will be proposed elsewhere.

Motivated by the above discussion, here we consider the following dimensionless *periodic* initial value problem for the *defocusing* NLS equation

$$i\epsilon q_t + \epsilon^2 q_{xx} - 2|q|^2 q = 0, \quad (1)$$

with initial conditions

$$q(x, 0) = \cos x, \quad -\pi \leq x \leq \pi. \quad (2)$$

The variables x and t are typically space and time, respectively (e.g., see [48, 49]), though in nonlinear fiber optics they have the reversed role of retarded time and propagation distance [29, 30, 50], and ϵ quantifies the smallness of dispersion [29] (in quantum-mechanical settings ϵ is also proportional to Planck's constant \hbar [24]) compared to the strength of nonlinear effects. Without loss of generality (taking advantage of the scaling invariances of Eq. (1)), we have normalized the period X_p of the cosine initial value to 2π .

The nonlinearity in Eq. (1) induces conversion towards high-frequency modes, i.e. odd harmonics $\pm m/X_p$, $m = 3, 5, \dots$ of the $m = 1$ input frequencies, a phenomenon commonly known in nonlinear optics as multiple four-wave mixing (mFWM) [30, 51, 52]. In the regime of interest here, $\epsilon \ll 1$, mFWM becomes very efficient and causes strong steepening of the cosine fronts, until breaking (hydrodynamic instability [29]) occurs followed by fission into soliton-like excitations, as shown by the numerical simulation in Fig. 1. Marked differences with the corresponding phenomena in the KdV equation [12, 19] are the degenerate mechanism for breaking that occurs at the null (vacuum) points (cf. [28, 31], where similar mechanism is analysed in detail for dark type input on a constant background) and the fission into pairs with opposite velocities, which reflect the bidirectional (NLS) versus unidirectional (KdV) dispersive hydrodynamic nature of such models [23]. Nevertheless, even in the NLS equation, solitons eventually give rise to a near-recurrence as shown in Fig. 1. Our goal, here, is to provide a quantitative description of this phenomenon, including analytical estimates of the

number of fissioning solitons and their velocities as a function of ϵ , and then use these results to characterise the recurrent behavior.

The outline of this work is the following. In section II we characterize the spectrum of the NLS equation (1) in the small dispersion limit with initial conditions (2) using a suitable WKB expansion. In section III we study the properties of the effective solitons arising from the corresponding spectrum. In section IV we discuss the recurrence of initial conditions. Section V offers a few concluding remarks. The details of the calculations are given in the Appendix.

II. NLS SPECTRUM IN THE SMALL DISPERSION LIMIT

II.1 Scattering problem and monodromy matrix

Since the NLS Eq. (1) is completely integrable, the initial value problem can be solved via the inverse scattering transform (IST). In particular, the relevant formalism here is the IST with periodic boundary conditions, or finite-gap theory [53–56]. According to the periodic IST, the nonlinear excitations embedded in the initial datum are encoded in the spectrum of the scattering problem associated with the NLS equation (1), i.e. the well-known Zakharov-Shabat (ZS) with cosine potential

$$\epsilon \phi_x = (-ik\sigma_3 + \cos x \sigma_1) \phi, \quad (3)$$

where $\phi(x, k) = (\phi_1, \phi_2)^T$ is the vector eigenfunction, and σ_1 and σ_3 are the first and third Pauli matrices, respectively. Since the scattering problem (3) is self-adjoint, all eigenvalues k are real. Applying the change of variables $v = \phi_1 + \phi_2$ and $\tilde{v} = \phi_1 - \phi_2$, Eq. (3) can be reduced to the second-order ordinary differential equation,

$$-\epsilon^2 v_{xx} + (\cos^2 x - \epsilon \sin x) v = \lambda v, \quad (4)$$

which is the time-independent Schrödinger equation with an ϵ -dependent potential and eigenvalue $\lambda = k^2 \geq 0$. Since the potential is periodic, Bloch-Floquet theory can be used to show that Eq. (4) admits bounded solutions if and only if

$$-2 \leq \text{tr} M \leq 2, \quad (5)$$

where $M(\lambda)$ is the monodromy matrix of the problem, defined as $M = Y^{-1}(-\pi)Y(\pi)$, and $Y(x)$ is any fundamental matrix solution of Eq. (4). The values of λ for which Eq. (5) is satisfied comprise the spectrum of Eq. (4). Note that, to each nonzero value of λ , there correspond two values $k = \pm\sqrt{\lambda}$ in the original scattering problem (3).

II.2 Wentzel-Kramers-Brillouin (WKB) analysis

Since no solutions in closed form are available for Eq. (4), we apply the WKB method (e.g., see [57]) to obtain asymptotic expansions for the solutions of Eq. (4) and therefore for

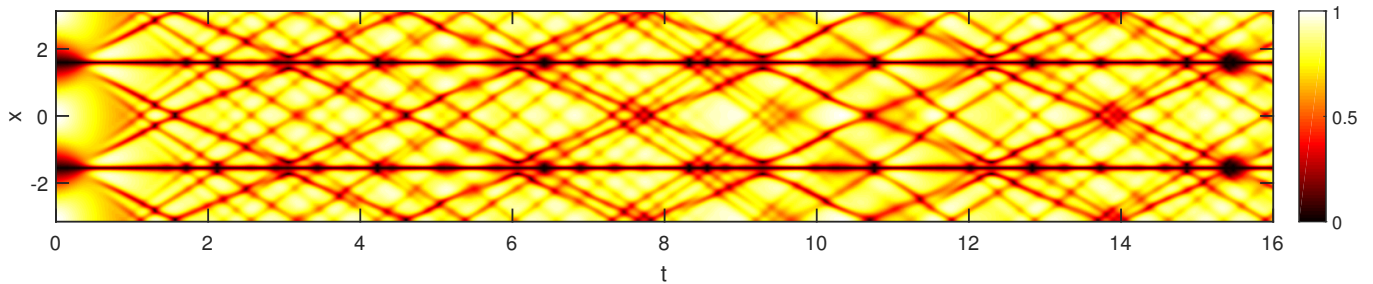


FIG. 1. Density plot of $|q(x,t)|$ from numerical solution of the initial value problem in Eqs. (1–2) with $\epsilon = 0.1$, showing the fission into soliton-like excitations as a result of breaking (hydrodynamic-like instability, see early stage $t < 1$) occurring in the null points of the input cosine and the following near-recurrence at $t \simeq 15.5$.

$\text{tr}M$ in the dispersionless limit, similarly to the approach developed in Refs. [19, 58]. It is convenient to introduce the shorthand notation

$$Q(x) = \lambda - \cos^2 x. \quad (6)$$

For $\lambda > 1$, no turning points are present, and straightforward calculations (see Appendix A.1 for details) yield

$$\text{tr}M = 2 \cos(S_0(\lambda)/\epsilon), \quad \lambda > 1, \quad (7a)$$

where $S_0(\lambda) = \int_{-\pi}^{\pi} \sqrt{Q(x)} dx$. On the other hand, for $0 < \lambda < 1$ four turning points are present, and the WKB analysis is considerably more complicated. In this case, the main difficulty comes from the fact that one must first construct asymptotic solutions in each of the regions away from the turning points and near each turning points, and then match the solutions in the transition regions around the turning points, obtaining so-called connection formulae which allow one to continue the asymptotic expressions for the eigenfunctions over the whole spatial domain. These expressions can then be used to finally construct the monodromy matrix. Omitting the details for brevity (see Appendix A.2 for details), we find the following expression for the trace of the monodromy matrix

$$\text{tr}M = 2 - 4 \sin^2(S_1(\lambda)/\epsilon) \cosh^2[S_{2,\epsilon}(\lambda)/\epsilon], \quad 0 < \lambda < 1, \quad (7b)$$

where $S_{2,\epsilon}(\lambda) = S_2(\lambda) + \epsilon \log 2$,

$$S_1(\lambda) = \int_c^{\pi-c} \sqrt{Q(x)} dx, \quad (8a)$$

$$S_2(\lambda) = \int_{-c}^c \sqrt{|Q(x)|} dx, \quad (8b)$$

and $c = \arccos(\sqrt{\lambda})$.

In the following, we conveniently refer to the half trace $\frac{1}{2}\text{tr}M$, which, according to Eqs. (7), turns out to be bounded by the unit value, i.e. $\frac{1}{2}\text{tr}M \leq 1$, for all $\lambda \geq 0$. In particular, Eq. (7a) shows that the range $1 < \lambda < \infty$ forms one infinitely long band. Conversely, Eq. (7b) shows that the range $0 \leq$

$\lambda < 1$ is divided into alternating bands and gaps corresponding to the values of λ for which $-1 \leq \frac{1}{2}\text{tr}M \leq 1$ (bands) or $\frac{1}{2}\text{tr}M < -1$ (gaps), respectively. The bands and gaps are separated by a sequence of band edges λ_n for $n = 0, 1, 2, \dots$, which are the values of λ such that $\frac{1}{2}\text{tr}M = -1$. Note that the value $\lambda = 0$ is always part of the spectrum (this can be seen by noting that for $k = 0$ the scattering problem decouples in the variables v and \tilde{v} , and can be solved exactly to get $\frac{1}{2}\text{tr}M = 1$, which coincides with the limiting value of Eq. (7b) as $k \rightarrow 0$).

As an example, in Fig. 2 (left panel) we show the dependence of $\frac{1}{2}\text{tr}M$ on the spectral parameter λ for $\epsilon = 0.15$. Note that, since $\text{tr}M$ exhibits exponentially large oscillations, to capture the whole behavior in a single plot we plot the quantity $f(\text{tr}M/2)$ instead of $\frac{1}{2}\text{tr}M$ itself, as in [59], with $f(\Delta)$ defined as $f(\Delta) = \Delta$ for $|\Delta| \leq 1$ and $f(\Delta) = \text{sign}(\Delta) (1 + \log_{10} |\Delta|)$ for $|\Delta| > 1$. In such figure we compare the above WKB asymptotic expressions for $\frac{1}{2}\text{tr}M$ in Eq. (7) with the values obtained from direct numerical integration of Eq. (4). As can be seen from the figure, the difference between the asymptotic expressions and the numerical values is negligible for our purposes.

III. EFFECTIVE SOLITONS

III.1 Asymptotic properties of the spectrum

Equation (7b) implies that, for $0 \leq \lambda < 1$, each band is clustered around a maximum of $\frac{1}{2}\text{tr}M$, at which $\frac{1}{2}\text{tr}M(\lambda) = 1$, and that the n -th maximum $\lambda = z_n$ is given by the solution of

$$S_1(z_n) = n\pi\epsilon. \quad (9)$$

Since $\lambda = k^2$, all spectral bands of the scattering problem (4) correspond to a symmetric pair of nonlinear excitations of the NLS Eq. (1) except for the first spectral band, centered around $k = 0$, which generates just one nonlinear excitation. Hence, the number N_e of nonlinear excitations of the problem is related to the total number N_b of spectral bands in the range $0 \leq \lambda < 1$ by $N_e = 2N_b - 1$. Since $S_1(1) = 2$, Eq. (9) then yields $N_b = \lfloor 2/(\pi\epsilon) \rfloor + 1$ and therefore $N_e =$

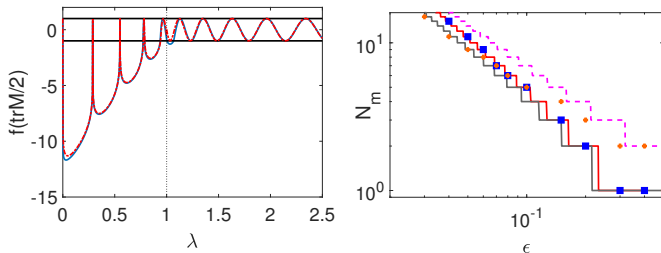


FIG. 2. Left panel: Half trace of the monodromy matrix $\frac{1}{2}\text{tr}M$ as a function of the eigenvalue λ with $\epsilon = 0.15$, comparing the asymptotic expressions (7) (dashed red) with the results from numerical integration of the scattering problem (4) (solid blue). Right panel: the number N_m of solitonic excitations as a function of ϵ . Red curve: full WKB prediction, Eq. (12). Gray curve: linear approximation, Eq. (13a). Blue squares: the value obtained from numerical integration of Eq. (3). Orange stars: same from direct numerical integration of Eq. (1). Also shown for comparison (magenta curve) is the total number of excitations N_e .

$2\lfloor 2/(\pi\epsilon) \rfloor + 1$. It was conjectured in [29, 30] that these excitations display soliton-like behavior. For a fixed value of ϵ , however, only some of the excitations in the problem resemble the dark solitons of the defocusing NLS equation. Note however that counting the number of excitations from direct numerical simulations of the NLS equation presents two major challenges. The first one is that not all excitations might be identifiable in the output. The second one is that it is highly nontrivial to distinguish which ones among all visible excitations are of solitonic or non-solitonic type. In order to distinguish soliton-like excitations from non-solitonic ones, one must look at the relative width $W_n = w_n/(w_n + g_n)$ of the n -th band, where w_n (g_n) is the width of n -th band (adjacent gap). By expanding the expression for $\text{tr}M$ in Eq. (7b), we find (see Appendix A.3 for details)

$$W_n = \frac{2}{\pi} \exp(-S_2(z_n)/\epsilon) + O(\epsilon e^{-S_2(z_n)/\epsilon}). \quad (10)$$

The proper solitonic limit of each excitation is obtained when the relative bandwidth W_n tends to zero. Of course, since the bandwidths are always greater than zero, one never has true solitons in the periodic problem. (This is at variance, for instance, with what happens when one considers the dark potential $q(x, t = 0) = \tanh x$ on the infinite line, which is reflectionless for integer $1/\epsilon$, containing a number $N_s = 2/\epsilon - 1$ of discrete eigenvalues that correspond to true solitons, as shown in [60].) Nonetheless, excitations associated with very narrow relative bandwidths ($W_n \ll 1$) become closer and closer approximations of the dark solitons of the defocusing NLS equation. Correspondingly, given a fixed threshold $\kappa \ll 1$, similarly to [19, 58] we define a nonlinear excitation of the periodic problem to be an *effective soliton* if the band to which it is associated is such that $W_n < \kappa$. Using Eq. (10) and solving this inequality, we then see that the solitonic bands are confined to the range $[0, \lambda_s)$, where λ_s is

defined by

$$S_2(\lambda_s) = \epsilon \log[2/(\pi\kappa)]. \quad (11)$$

Denoting by N_m the total number of maxima in $[0, \lambda_s)$, we have that N_m is also the number of *distinct soliton pairs* (in which any two symmetric gray solitons are counted as one, like the lone black soliton). In light of the above discussion, from Eq. (9) we then have

$$N_m = \lfloor S_1(\lambda_s)/(\pi\epsilon) + 1 \rfloor. \quad (12)$$

The total number of solitons present in the problem is then simply $N_s = 2N_m - 1$. As shown in Fig. 2 (right panel), the above WKB estimate for the total number of solitons is in excellent agreement with results from numerical integration of Eq. (3) and also in good agreement with direct numerical simulations of Eq. (1) (again with the caveat regarding the difficulty of counting numerically the number of excitations in case of small dispersion).

We can also derive *fully explicit* approximations for the number of solitons as a function of ϵ by considering either a linear or quadratic expansion of $S_1(\lambda)$ near $\lambda = 0$ and a linear expansion of $S_2(\lambda)$ near $\lambda = 1$ (see Appendix A.3 for details), thus obtaining

$$N_{m,\text{linear}} = \left\lfloor \frac{1}{2\epsilon} - \frac{1}{\pi} \log \frac{2}{\pi\kappa} + 1 \right\rfloor, \quad (13a)$$

$$N_{m,\text{quadratic}} = \left\lfloor \frac{4\sqrt{2} + 1}{8\sqrt{2}\epsilon} - \frac{2\sqrt{2} + 1}{2\sqrt{2}\pi} \log \frac{2}{\pi\kappa} + 1 \right\rfloor, \quad (13b)$$

respectively. Corresponding approximations for N_s follow accordingly. The values of $N_{m,\text{linear}}$ are shown in Fig. 2; those of $N_{m,\text{quadratic}}$ are almost indistinguishable from the “exact” count given by Eq. (12). Note that in both cases the leading order term is independent of the specific value chosen for the threshold κ .

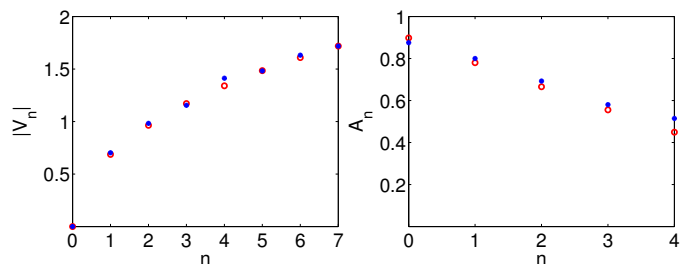


FIG. 3. Absolute value of the soliton velocity $|V_n|$ (left panel) and amplitude A_n (right panel) for the soliton set associated to a given index n . Red circles: asymptotic values; Blue dots: direct numerical simulations of Eqs. (1)-(2). Here $\epsilon = 0.06$, resulting in $N_s = 15$ and $q_\infty = 0.898$.

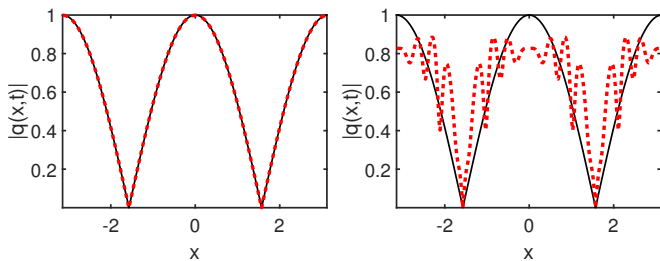


FIG. 4. Near-recurrence of initial condition for $\epsilon = 0.3$ (left panel) and $\epsilon = 0.08$ (right panel), comparing the initial value (2) (solid black) and $q(x, t)$ at the near-recurrence time (dashed red).

III.2 Amplitudes and velocities of the effective solitons

Recall that the single dark-soliton solution of the defocusing NLS equation associated with a discrete eigenvalue $k = k_0$ is such that

$$|q(x, t)|^2 = k_0^2 + (q_\infty^2 - k_0^2) \tanh^2[\sqrt{q_\infty^2 - k_0^2}(x - x_0 - 2k_0t)], \quad (14)$$

where $q_\infty = \lim_{x \rightarrow \pm\infty} |q(x, t)|$ is the background amplitude. Also recall that, to each solitonic band centered at $\lambda = z_n \neq 0$, with z_n defined by Eq. (9), there corresponds a pair of dark solitons with discrete eigenvalues $k_{\pm n} = \pm\sqrt{z_n}$. The band centered at $z_0 = 0$, instead, corresponds to a single black soliton. We then obtain the velocity and the amplitude of the n -th set of solitons as $V_n = \pm 2\sqrt{z_n}$ and $A_n = q_\infty^2 - z_n$, respectively, $n = 0, 1, 2, \dots$. Finally, recall that, in the infinite line problem, the continuous spectrum is $k \in (-\infty, -q_\infty) \cup (q_\infty, \infty)$. Identifying the beginning of the continuous spectrum with the first non-solitonic band, we therefore have $q_\infty = \sqrt{z_{N_m+1}}$. Figure 3 shows a comparison between the above WKB estimates for the soliton velocities and amplitudes and the values obtained from direct numerical simulations of the NLS equation.

IV. RECURRENCE OF INITIAL CONDITIONS

Similarly to the KdV equation, the evolution ruled by the defocusing NLS equation is expected to nearly recover the cosine initial value when the solitons simultaneously return to their initial location after traveling an integer number of periods.

Figure 4 shows the solution at the (numerically determined) recurrence time for $\epsilon = 0.3$ and $\epsilon = 0.08$. The numerically determined dependence of the recurrence time on ϵ is also shown in Fig. 5. Next we show how one can use the above WKB results to obtain an estimate of the recurrence time, where we neglect the small shifts due to soliton collisions.

Since our purpose is also to study the differences between recurrences in the KdV and the NLS equations, let us briefly

consider first the case of the KdV, which we write as

$$u_t + 6uu_x + \epsilon^2 u_{xxx} = 0. \quad (15)$$

An estimate for the recurrence time in Eq. (15) can be obtained from the WKB analysis developed in Refs. [19, 58]. Adopting the same notation of such references, we recall that, in this case, the solitonic bands correspond to nonlinear excitations that are close to bright KdV solitons of the form

$$u_n(x, t) = u_0 + A_n \operatorname{sech}^2[\sqrt{A_n/2}(x - V_n t)/\epsilon], \quad (16)$$

where A_n is the amplitude of the n -th soliton from the background level u_0 , and $V_n = 6u_0 + 2A_n$ is the corresponding velocity. The amplitude can be calculated as [58, 59] $A_n = 2(\lambda_{\text{ref}} - \lambda_n)$ for $n = 1, 2, \dots, N$, where N is the number of the solitonic bands and $\lambda_{\text{ref}} = -u_0$ corresponds to the $(N + 1)$ -th band, or first non-solitonic band. According to the analysis in Ref. [58] and adopting a linear approximation for the eigenvalues, we find that the amplitudes and hence the velocities scales linearly with the soliton order n , with increment $\Delta A = A_n - A_{n+1} = 2\sqrt{2}\epsilon$ and hence $\Delta V = V_n - V_{n+1} = 4\sqrt{2}\epsilon$. Clearly, this means that after a time T_{KdV} such that $\Delta V T_{\text{KdV}} = 2\pi$, all the solitons recur having traveled a multiple of the period (recall that 2π is the period of the cosine, and note that, obviously, the contribution to the velocity that is common to all solitons does not affect the recurrence time). From this condition we then immediately find

$$T_{\text{KdV}} = \frac{\pi}{2\sqrt{2}\epsilon}. \quad (17)$$

Remarkably, the estimate in Eq. (17) coincides with an earlier one by Toda [15, 16] (once one performs the trivial rescalings of the spatial and temporal variables so as to obtain the same form of the KdV equation). We note, however, that Toda's estimate was obtained using a quadratic (parabolic) approximation for the cosine potential, which amounts to approximating the eigenvalues with those of an harmonic oscillator. Importantly, numerical results (not shown) based on the integration of the KdV equation confirm the scaling of the recurrence time with ϵ^{-1} from Eq. (17), while the recurrence times from the numerics turn out to be slightly overestimated by the formula, possibly due to the soliton-soliton interactions, which are neglected in both our and Toda's approaches.

Returning back to the defocusing NLS equation, the time needed for the n -th soliton pair to travel a distance equal to a whole period is $T_n = 2\pi/|V_n|$, with $V_n = \pm 2\sqrt{z_n}$ as before. By employing again a linear expansion of $S_1(\lambda)$ around $\lambda = 0$ (see Eqs. (35a) in Appendix), we obtain the explicit expression $V_n = \pm 2\sqrt{2n\epsilon}$, which in turn yields

$$T_n = \frac{\pi}{\sqrt{2n\epsilon}}. \quad (18)$$

This result shows that the key difference between the NLS and KdV equations is that, for the latter, V_n is linearly proportional

to the soliton index n (in the WKB limit), whereas the above expression shows that for the NLS solitons V_n depends on the square root of n . This difference is reflected in the travel time T_n . Therefore, while in the KdV equation all solitons simultaneously return to their initial position at the recurrence time, this is not true in the NLS equation, and the situation is more complicated in this case.

More precisely, neglecting the interaction-induced position shifts, for any fixed integer $m > 0$, all soliton pairs with indices $n = m, 4m, 9m, \dots, l^2m, \dots$ (with l any fixed positive integer) will return to their initial position, which is also the position of the stationary black soliton, at integer multiples of the recurrence time $t_{Rm} = \pi/\sqrt{2m\epsilon}$. The value of t_{R1} as a function of ϵ , shown in Fig. 5, is in good agreement with the numerically determined recurrence times. Importantly, note that the recurrence time for the NLS equation scales like $\epsilon^{-1/2}$, whereas the recurrence time for the KdV equation scales like ϵ^{-1} .

In order to further characterise the degree of the recurrence, we introduce the following figure of merit

$$R = 1 - \frac{\| |q(x, t)| - |\cos x| \|}{\| \cos x \|}, \quad (19)$$

where $\|f\|^2 = \int_0^{2\pi} |f(x)|^2 dx$ quantifies the energy contained in a periodic signal. (Note that $\| \cos x \|^2 = \pi$.) The value of R is a measure of the strength of the recurrence. A perfect recurrence corresponds to $R = 1$. The numerically determined dependence of R on ϵ is reported in Fig. 5, showing a strong deterioration for decreasing ϵ , whereas near-perfect recurrence is achieved for relatively large values of ϵ . The latter fact is straightforwardly explained from Eq. (12), which implies that, for $\epsilon > 0.163$, there is only one soliton pair besides the stationary black soliton. In this regime, the initial condition is recovered almost exactly at multiples of $t_R = \pi/(\sqrt{2\epsilon})$, as also illustrated in Fig. 4 (left panel), consistently with earlier experiments [61, 62] (see also [29]). However, for $\epsilon < 0.163$, multiple soliton pairs come into play, and the recurrence becomes progressively worse for decreasing ϵ , as illustrated for $\epsilon = 0.08$ in Fig. 4 (right panel). Importantly, a similar calculation for the KdV equation also shows a recurrence degradation with decreasing ϵ . However, the scaling law in the two models is different. Specifically, R scales proportionally to ϵ for the KdV, and as $\epsilon^{1/4}$ for the NLS (see Fig. 4, right panel). No analytical results are available in either model which explain this dependence.

V. CONCLUSIONS

In summary, we have shown that, in systems governed by the weakly dispersing defocusing NLS equation, the fission of solitons from a periodic wave and their recurrence can be described in full analytical fashion. The result demonstrates that the phenomenon of near-recurrence discovered by ZK is observable in other integrable systems, though important differences arise due to the different scaling of soliton velocities with their order. We believe that our approach can be

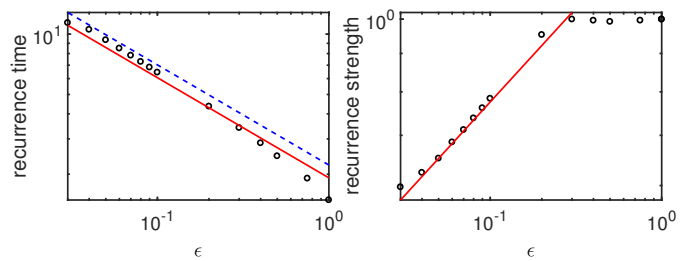


FIG. 5. Left panel: recurrence time as a function of ϵ , as computed from direct numerical simulations of Eqs. (1)-(2) (black circles), along with a linear fit of the numerical data (red line) and the analytical prediction $t_{\text{recur}} = t_{R1}$ (dashed blue line). Right panel: Figure of merit of recurrence strength [Eq. (19)], as computed from direct numerical simulations (black circles), and its linear fit for $\epsilon < 0.3$ (red line).

easily extended to other integrable systems (e.g., such as the Benjamin-Ono equation) in order to produce a critical assessment on the general degree of universality of the recurrence phenomenon originally discussed by ZK for the KdV equation. We also expect our results to be experimentally verifiable in fiber optics (in the context of mFWM dynamics) and possibly in other settings (Bose-Einstein condensates, spin waves, oscillator chains).

The results of this work also open up the interesting question of whether a similar approach can also be used to study the small dispersion limit of the focusing NLS equation with periodic boundary conditions. Of course the focusing case is expected to be more challenging than the defocusing one. From a mathematical point of view, this is because the corresponding spectral problem is no longer self-adjoint, which means that the spectral bands are not restricted to the real axis, and which puts into question whether one can effectively make use of the WKB method. Physically, the problem is also expected to give rise to more complex phenomena because of the presence of modulational instability, which becomes more and more severe in the dispersionless limit (i.e., as $\epsilon \rightarrow 0$).

Acknowledgment. We thank A. Armaroli for insightful discussions during the early stage of this work. This work was supported in part by the National Science Foundation under grant numbers DMS-1614623 and DMS-1615524. S.T. acknowledges support from the Italian Ministry of University and Research (PRIN-2012BFNWZ2)

APPENDIX

Here we provide the details on the analytical calculation of the monodromy matrix and the relative bandwidths.

A.1 The WKB expansion and the range $\lambda > 1$

The WKB expansion. Recall that the scattering problem is given by Eq. (4). We look for an asymptotic expansion for the

solution v of Eq. (4) in the form

$$v(x) = [A(x) + O(\epsilon)] e^{iS(x)/\epsilon}, \quad (20)$$

as $\epsilon \rightarrow 0$. Substituting Eq. (20) into Eq. (4), one obtains, at the first two orders in the expansion, the eikonal equation and the transport equation, i.e.,

$$S_x^2 = Q(x), \quad (21a)$$

$$2iS_x A_x + iS_{xx} A + \sin x A = 0, \quad (21b)$$

respectively. These equations are readily integrated to obtain

$$S_{\pm}(x) = \pm \int \sqrt{Q(x)} dx, \quad (22a)$$

$$A_{\pm}(x) = \sqrt{\sqrt{Q(x)} \mp i \cos x} / \sqrt[4]{Q(x)}, \quad (22b)$$

up to arbitrary additive and multiplicative constants, respectively, where $Q(x) = \lambda - \cos^2 x$ was defined in Eq. (6), and A_{\pm} corresponds to the plus/minus sign in $S_{\pm}(x)$, respectively.

Observe that, for $\lambda > 1$, $Q(x) > 0$ for all $x \in R$. Conversely, for $0 < \lambda < 1$ the range $x \in [-\pi, \pi]$ divides into three sub-domains:

- (i) $Q(x) < 0$ for $x \in [-\pi, -c_2] \cup (-c_1, c_1) \cup (c_2, \pi]$,
- (ii) $Q(x) > 0$ for $x \in (-c_2, -c_1) \cup (c_1, c_2)$,
- (iii) $Q(x) = 0$ for $x = \pm c_1, \pm c_2$,

where $c_1 = \arccos(\sqrt{\lambda})$ and $c_2 = \pi - c_1$ (with $c = c_1$). We then need to study the WKB solutions in these two ranges of λ separately.

Trace of the monodromy matrix for $\lambda > 1$. For any value of λ in this range, $Q(x)$ is positive. Two linearly independent solutions are given, in the WKB approximation, by

$$v_{\pm}(x) = A_{\pm}(x) e^{iS_{\pm}(x)/\epsilon}, \quad (23)$$

with $A_{\pm}(x)$ and $S_{\pm}(x)$ given by Eq. (22). We can write a corresponding fundamental matrix solution of the first-order system associated with Eq. (4) as a Wronskian:

$$Y(x) = \text{Wr}(v_-, v_+). \quad (24)$$

Since $Q(x) \neq 0$ in this case, such a fundamental matrix solution is valid over the whole range $x \in [-\pi, \pi]$. Therefore the monodromy matrix can be obtained simply as

$$M = Y^{-1}(-\pi)Y(\pi). \quad (25)$$

Straightforward calculations then show that the trace of M is given by Eq. (7a).

A.2 Trace of the monodromy matrix for $0 < \lambda < 1$

WKB solutions for $0 < \lambda < 1$. For all values of λ in this range, there are four turning points, namely $\pm c_1, \pm c_2$. Correspondingly we need to discuss the behavior of the eigenfunctions in the following nine sub-regions of the fundamental period $x \in [-\pi, \pi]$:

- (a) Region 1, $x \in [-\pi, -c_2]$;
- (b) First transition region, comprised by a neighborhood of $x = -c_2$;
- (c) Region 2, $x \in (-c_2, -c_1)$;
- (d) Second transition region, comprised by a neighborhood of $x = -c_1$;
- (e) Region 3, $x \in (-c_1, c_1)$;
- (f) Third transition region, comprised by a neighborhood of $x = c_1$;
- (g) Region 4, $x \in (c_1, c_2)$;
- (h) Fourth transition region, comprised by a neighborhood of $x = c_2$;
- (i) Region 5, $x \in (c_2, \pi]$.

The various sub-regions are illustrated in Fig. 6. Next, we discuss the WKB solution of the scattering problem in the various sub-regions.

(a) In region 1, $x \in [-\pi, -c_2]$, the WKB approximation for the general solution of the scattering problem (4) is

$$v_1(x) = a_1^+ v_{1+}(x) + a_1^- v_{1-}(x), \quad (26)$$

where

$$v_{1\pm}(x) = A_{\pm} \exp(\mp \int_{-c_2}^x \sqrt{|Q(x)|} dx / \epsilon), \quad (27)$$

and

$$A_{\pm} = [\pm |Q(x)|^{1/2} - q]^{1/2} / |Q(x)|^{1/4}. \quad (28)$$

(b) In the first transition region, $x \in (-c_2 - \delta, -c_2 + \delta)$ with $\delta > 0$, Eq. (4) becomes

$$\epsilon^2 v_{xx} + (2k\sqrt{1-k^2}(x+c_2) - \epsilon\sqrt{1-k^2})v = 0,$$

an asymptotic expansion for v in the first transition region is given by

$$v_{1 \rightarrow 2}(x) = c_1^- \text{Ai}[\xi(x)] + c_1^+ \text{Bi}[\xi(x)],$$

where

$$\xi(x) = -a^{1/3}(x+c_2 - \epsilon/2k)/\epsilon^{2/3}, \quad a = 2k\sqrt{1-k^2}.$$

(c) In region 2, $x \in (-c_2, -c_1)$, the WKB approximation to the general solution has two equivalent expressions

$$v_2(x) = a_2^+ A_+(x) \exp(i \int_{-c_2}^x \sqrt{|Q(x)|} dx / \epsilon)$$

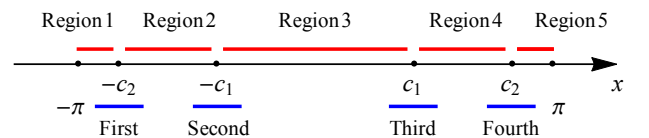


FIG. 6. The sub-regions of the fundamental domain $x \in [-\pi, \pi]$ for the WKB analysis in the range $0 < \lambda < 1$.

$$+ a_2^- A_-(x) \exp(-i \int_{-c_2}^x \sqrt{|Q(x)|} dx / \epsilon), \quad (29a)$$

$$v_2(x) = \bar{a}_2^+ A_+(x) \exp(i \int_{-c_1}^x \sqrt{|Q(x)|} dx / \epsilon) \\ + \bar{a}_2^- A_-(x) \exp(-i \int_{-c_1}^x \sqrt{|Q(x)|} dx / \epsilon), \quad (29b)$$

with A_{\pm} given by Eq. (22).

(d) In the second transition region, i.e., $x \in (-c_1 - \delta, -c_1 + \delta)$, Eq. (4) becomes

$$\epsilon^2 v_{xx} - (2k\sqrt{1-k^2}(x+c_1) + \epsilon\sqrt{1-k^2})v = 0.$$

An asymptotic expansion for v in the second transition region is given by

$$v_{2 \rightarrow 3}(x) = c_2^- \text{Ai}[\eta(x)] + c_2^+ \text{Bi}[\eta(x)],$$

where $\eta(x) = a^{1/3}(x+c_1 + \epsilon/2k)/\epsilon^{2/3}$.

(e) In region 3, $x \in (-c_1, c_1)$, the general solution in the WKB approximation also has two equivalent expressions

$$v_3(x) = a_3^+ A_+(x) \exp(- \int_{-c_1}^x \sqrt{|Q(x)|} dx / \epsilon) \\ + a_3^- A_-(x) \exp(\int_{-c_1}^x \sqrt{|Q(x)|} dx / \epsilon), \quad (30a)$$

$$v_3(x) = \bar{a}_3^+ A_+(x) \exp(- \int_{c_1}^x \sqrt{|Q(x)|} dx / \epsilon) \\ + \bar{a}_3^- A_-(x) \exp(\int_{c_1}^x \sqrt{|Q(x)|} dx / \epsilon), \quad (30b)$$

where $A_{\pm} = [\mp |Q(x)|^{1/2} + q]^{1/2} / |Q(x)|^{1/4}$.

(f) In the third transition region, $x \in (c_1 - \delta, c_1 + \delta)$, Eq. (4) becomes

$$\epsilon^2 v_{xx} + (2k\sqrt{1-k^2}(x-c_1) + \epsilon\sqrt{1-k^2})v = 0.$$

An asymptotic expansion for v in the third transition region is given by

$$v_{3 \rightarrow 4}(x) = c_3^- \text{Ai}[z(x)] + c_3^+ \text{Bi}[z(x)],$$

where $z(x) = -a^{1/3}(x-c_1 + \epsilon/2k)/\epsilon^{2/3}$.

(g) In Region 4, $x \in (c_1, c_2)$, the WKB approximation to the general solution again has two equivalent expressions

$$v_4(x) = a_4^+ A_+(x) \exp(i \int_{c_1}^x \sqrt{|Q(x)|} dx / \epsilon) \\ + a_4^- A_-(x) \exp(-i \int_{c_1}^x \sqrt{|Q(x)|} dx / \epsilon), \quad (31a)$$

$$v_4(x) = \bar{a}_4^+ A_+(x) \exp(i \int_{c_2}^x \sqrt{|Q(x)|} dx / \epsilon) \\ + \bar{a}_4^- A_-(x) \exp(-i \int_{c_2}^x \sqrt{|Q(x)|} dx / \epsilon), \quad (31b)$$

with A_{\pm} given by Eq. (22).

(h) In the fourth transition region, $x \in (c_2 - \delta, c_2 + \delta)$, Eq. (4) becomes

$$\epsilon^2 v_{xx} - (2k\sqrt{1-k^2}(x-c_2) - \epsilon\sqrt{1-k^2})v = 0,$$

an asymptotic expansion for v in the fourth transition region is given by

$$v_{4 \rightarrow 5}(x) = c_4^- \text{Ai}[\gamma(x)] + c_4^+ \text{Bi}[\gamma(x)],$$

where $\gamma(x) = a^{1/3}(x-c_2 - \epsilon/2k)/\epsilon^{2/3}$.

(i) In region 5, $x \in (c_2, \pi]$, the general solution in the WKB approximation is

$$v_5(x) = a_5^+ A_+(x) \exp(- \int_{c_2}^x \sqrt{|Q(x)|} dx / \epsilon) \\ + a_5^- A_-(x) \exp(\int_{c_2}^x \sqrt{|Q(x)|} dx / \epsilon),$$

with A_{\pm} given by Eq. (28).

Connection formulae for $0 < \lambda < 1$. Having computed WKB expressions for the solution of the scattering problem in the various sub-domains for $0 < \lambda < 1$, we now need to match the solutions across different sub-regions. First we match $v_1(x)$ with $v_{1 \rightarrow 2}(x)$. Explicitly,

$$v_1(x) = \frac{1}{\sqrt[4]{a|x+c_2|}} (a_1^+ \sqrt[4]{\lambda} e^{\frac{2}{3}\sqrt{a}|x+c_2|^{3/2}/\epsilon} \\ + a_1^- \sqrt[4]{\lambda} e^{-\frac{2}{3}\sqrt{a}|x+c_2|^{3/2}/\epsilon}) (1 + O(|x+c_2|)), \\ x \rightarrow -c_2, \\ v_{1 \rightarrow 2}(x) = \frac{1}{\sqrt[4]{\pi^2 \xi}} (\frac{1}{2} c_1^- e^{-\frac{2}{3}\xi^{3/2}} + c_1^+ e^{\frac{2}{3}\xi^{3/2}}) \\ \times (1 + O(1/\xi^{3/2})), \quad \xi \rightarrow \infty.$$

Requiring that these two expansions match, we obtain the connection formula

$$\begin{pmatrix} c_1^- \\ c_1^+ \end{pmatrix} = C_1 \begin{pmatrix} a_1^- \\ a_1^+ \end{pmatrix}, \quad C_1 = \frac{\sqrt[4]{\pi^2 \lambda}}{(a\epsilon)^{1/6}} \begin{pmatrix} 2 & 0 \\ 0 & 1 \end{pmatrix}.$$

To match $v_2(x)$ with $v_{1 \rightarrow 2}(x)$, note that

$$v_2(x) = \frac{1}{\sqrt[4]{a(x+c_2)}} (a_2^+ \sqrt[4]{\lambda} e^{i\pi/4} e^{\frac{2}{3}i\sqrt{a}(x+c_2)^{3/2}/\epsilon} \\ + a_2^- \sqrt[4]{\lambda} e^{-i\pi/4} e^{-\frac{2}{3}i\sqrt{a}(x+c_2)^{3/2}/\epsilon}) (1 + O(x+c_2)), \\ x \rightarrow -c_2,$$

$$v_{1 \rightarrow 2}(x) = \frac{1}{\sqrt[4]{\pi^2 |\xi|}} [c_1^- \sin(\frac{2}{3}|\xi|^{3/2} + \frac{\pi}{4}) \\ + c_1^+ \cos(\frac{2}{3}|\xi|^{3/2} + \frac{\pi}{4})] (1 + O(1/|\xi|^{3/2})), \quad \xi \rightarrow -\infty,$$

implying

$$\begin{pmatrix} a_2^+ \\ a_2^- \end{pmatrix} = C_2 \begin{pmatrix} c_1^- \\ c_1^+ \end{pmatrix}, \quad C_2 = \frac{(a\epsilon)^{1/6}}{2\sqrt[4]{\pi^2 \lambda}} \begin{pmatrix} -i & 1 \\ i & 1 \end{pmatrix}.$$

Note also that \bar{a}_2^\pm in Eq. (29b) relates to a_2^\pm in Eq. (29a) by

$$\begin{pmatrix} \bar{a}_2^+ \\ \bar{a}_2^- \end{pmatrix} = C_3 \begin{pmatrix} a_2^+ \\ a_2^- \end{pmatrix}, \quad C_3 = e^{i\sigma_3 S_1(\lambda)/\epsilon},$$

with

$$S_1(\lambda) = \int_{c_1}^{c_2} \sqrt{Q(x)} dx. \quad (32)$$

A plot of $S_1(\lambda)$ is shown in Fig. 7.

Next we match $v_2(x)$ with $v_{2 \rightarrow 3}(x)$. Note that

$$\begin{aligned} v_2(x) &= \frac{1}{\sqrt[4]{a|x+c_1|}} (\bar{a}_2^- \sqrt[4]{\lambda} e^{i\pi/4} e^{\frac{2}{3}i\sqrt{a}|x+c_1|^{3/2}/\epsilon} \\ &+ \bar{a}_2^+ \sqrt[4]{\lambda} e^{-i\pi/4} e^{-\frac{2}{3}i\sqrt{a}|x+c_1|^{3/2}/\epsilon}) (1 + O(x+c_1)), \\ x &\rightarrow -c_1, \end{aligned}$$

$$\begin{aligned} v_{2 \rightarrow 3}(x) &= \frac{1}{\sqrt[4]{\pi^2|\eta|}} [c_2^- \sin(\frac{2}{3}|\eta|^{3/2} + \frac{\pi}{4}) \\ &+ c_2^+ \cos(\frac{2}{3}|\eta|^{3/2} + \frac{\pi}{4})] (1 + O(1/|\eta|^{3/2})), \quad \eta \rightarrow -\infty. \end{aligned}$$

Requiring that these two expansions match, we obtain the connection formula

$$\begin{pmatrix} c_2^+ \\ c_2^- \end{pmatrix} = C_4 \begin{pmatrix} \bar{a}_2^+ \\ \bar{a}_2^- \end{pmatrix}, \quad C_4 = \frac{\sqrt[4]{\pi^2\lambda}}{(a\epsilon)^{1/6}} \begin{pmatrix} 1 & 1 \\ -i & i \end{pmatrix}.$$

Next we match $v_3(x)$ with $v_{2 \rightarrow 3}(x)$. Note that

$$\begin{aligned} v_3(x) &= \frac{1}{\sqrt[4]{a(x+c_1)}} (a_3^- \sqrt[4]{\lambda} e^{\frac{2}{3}\sqrt{a}(x+c_1)^{3/2}/\epsilon} \\ &+ a_3^+ \sqrt[4]{\lambda} e^{-\frac{2}{3}\sqrt{a}(x+c_1)^{3/2}/\epsilon}) (1 + O(x+c_1)), \\ x &\rightarrow -c_1, \end{aligned}$$

$$\begin{aligned} v_{2 \rightarrow 3}(x) &= \frac{1}{\sqrt[4]{\pi^2\eta}} (\frac{1}{2}c_2^- e^{-\frac{2}{3}\eta^{3/2}} + c_2^+ e^{\frac{2}{3}\eta^{3/2}}) \\ &\times (1 + O(1/\eta^{3/2})), \quad \eta \rightarrow \infty. \end{aligned}$$

Matching these expansions, we obtain

$$\begin{pmatrix} a_3^- \\ a_3^+ \end{pmatrix} = C_5 \begin{pmatrix} c_2^+ \\ c_2^- \end{pmatrix}, \quad C_5 = \frac{(a\epsilon)^{1/6}}{\sqrt[4]{\pi^2\lambda}} \begin{pmatrix} 1 & 0 \\ 0 & \frac{1}{2} \end{pmatrix}.$$

Note that \bar{a}_3^\pm in Eq. (30b) relates to a_3^\pm in Eq. (30a) by

$$\begin{pmatrix} \bar{a}_3^- \\ \bar{a}_3^+ \end{pmatrix} = C_6 \begin{pmatrix} a_3^- \\ a_3^+ \end{pmatrix}, \quad C_6 = e^{\sigma_3 S_2(\lambda)/\epsilon}$$

with

$$S_2(\lambda) = \int_{c_2}^{c_3} \sqrt{|Q(x)|} dx. \quad (33)$$

A plot of $S_2(\lambda)$ is shown in Fig. 7.

To match $v_3(x)$ with $v_{3 \rightarrow 4}(x)$, note that

$$\begin{aligned} v_3(x) &= \frac{1}{\sqrt[4]{a|x-c_1|}} (\bar{a}_3^+ \sqrt[4]{\lambda} e^{\frac{2}{3}\sqrt{a}|x-c_1|^{3/2}/\epsilon} \\ &+ \bar{a}_3^- \sqrt[4]{\lambda} e^{-\frac{2}{3}\sqrt{a}|x-c_1|^{3/2}/\epsilon}) (1 + O(|x-c_1|)), \\ x &\rightarrow c_1, \end{aligned}$$

$$\begin{aligned} v_{3 \rightarrow 4}(x) &= \frac{1}{\sqrt[4]{\pi^2 z}} (\frac{1}{2}c_3^- e^{-\frac{2}{3}z^{3/2}} + c_3^+ e^{\frac{2}{3}z^{3/2}}) \\ &\times (1 + O(1/z^{3/2})), \quad z \rightarrow \infty. \end{aligned}$$

Requiring that these two expansions match, we obtain the connection formula

$$\begin{pmatrix} c_3^- \\ c_3^+ \end{pmatrix} = C_1 \begin{pmatrix} \bar{a}_3^- \\ \bar{a}_3^+ \end{pmatrix}.$$

Next we match $v_4(x)$ with $v_{3 \rightarrow 4}(x)$, note that

$$\begin{aligned} v_4(x) &= \frac{1}{\sqrt[4]{a(x-c_1)}} (a_4^+ \sqrt[4]{\lambda} e^{-i\pi/4} e^{\frac{2}{3}i\sqrt{a}(x-c_1)^{3/2}/\epsilon} \\ &+ a_4^- \sqrt[4]{\lambda} e^{i\pi/4} e^{-\frac{2}{3}i\sqrt{a}(x-c_1)^{3/2}/\epsilon}) (1 + O(x-c_1)), \\ x &\rightarrow c_1, \end{aligned}$$

$$\begin{aligned} v_{3 \rightarrow 4}(x) &= \frac{1}{\sqrt[4]{\pi^2|z|}} [c_3^- \sin(\frac{2}{3}|z|^{3/2} + \frac{\pi}{4}) \\ &+ c_3^+ \cos(\frac{2}{3}|z|^{3/2} + \frac{\pi}{4})] (1 + O(1/|z|^{3/2})), \quad z \rightarrow -\infty. \end{aligned}$$

Matching these expansions, we obtain

$$\begin{pmatrix} a_4^+ \\ a_4^- \end{pmatrix} = C_7 \begin{pmatrix} c_3^- \\ c_3^+ \end{pmatrix}, \quad C_7 = \frac{(a\epsilon)^{1/6}}{2\sqrt[4]{\pi^2\lambda}} \begin{pmatrix} 1 & i \\ 1 & -i \end{pmatrix}.$$

Note also that \bar{a}_4^\pm in Eq. (31b) relates to a_4^\pm in Eq. (31a) by

$$\begin{pmatrix} \bar{a}_4^+ \\ \bar{a}_4^- \end{pmatrix} = C_3 \begin{pmatrix} a_4^+ \\ a_4^- \end{pmatrix}.$$

Then we match $v_4(x)$ with $v_{4 \rightarrow 5}(x)$. Note that

$$\begin{aligned} v_4(x) &= \frac{1}{\sqrt[4]{a|x-c_2|}} (\bar{a}_4^- \sqrt[4]{\lambda} e^{-i\pi/4} e^{\frac{2}{3}i\sqrt{a}|x-c_2|^{3/2}/\epsilon} \\ &+ \bar{a}_4^+ \sqrt[4]{\lambda} e^{i\pi/4} e^{-\frac{2}{3}i\sqrt{a}|x-c_2|^{3/2}/\epsilon}) (1 + O(x-c_2)), \\ x &\rightarrow c_2, \end{aligned}$$

$$\begin{aligned} v_{4 \rightarrow 5}(x) &= \frac{1}{\sqrt[4]{\pi^2|\gamma|}} [c_4^- \sin(\frac{2}{3}|\gamma|^{3/2} + \frac{\pi}{4}) \\ &+ c_4^+ \cos(\frac{2}{3}|\gamma|^{3/2} + \frac{\pi}{4})] (1 + O(1/|\gamma|^{3/2})), \quad \gamma \rightarrow -\infty. \end{aligned}$$

Requiring that these two expansions match, we obtain the connection formula

$$\begin{pmatrix} c_4^+ \\ c_4^- \end{pmatrix} = C_8 \begin{pmatrix} \bar{a}_4^+ \\ \bar{a}_4^- \end{pmatrix}, \quad C_8 = \frac{\sqrt[4]{\pi^2\lambda}}{(a\epsilon)^{1/6}} \begin{pmatrix} i & -i \\ 1 & 1 \end{pmatrix}.$$

Finally we match $v_5(x)$ with $v_{4 \rightarrow 5}(x)$. Note that

$$\begin{aligned} v_5(x) &= \frac{1}{\sqrt[4]{a(x-c_2)}} (a_5^- \sqrt[4]{\lambda} e^{\frac{2}{3}\sqrt{a}(x-c_2)^{3/2}/\epsilon} \\ &+ a_5^+ \sqrt[4]{\lambda} e^{-\frac{2}{3}\sqrt{a}(x-c_2)^{3/2}/\epsilon}) (1 + O(x-c_2)), \\ x &\rightarrow c_2, \end{aligned}$$

$$\begin{aligned} v_{4 \rightarrow 5}(x) &= \frac{1}{\sqrt[4]{\pi^2\gamma}} (\frac{1}{2}c_4^- e^{-\frac{2}{3}\gamma^{3/2}} + c_4^+ e^{\frac{2}{3}\gamma^{3/2}}) \\ &\times (1 + O(1/\gamma^{3/2})), \quad \gamma \rightarrow \infty. \end{aligned}$$

Matching these expansions, we obtain

$$\begin{pmatrix} a_5^- \\ a_5^+ \end{pmatrix} = C_5 \begin{pmatrix} c_4^+ \\ c_4^- \end{pmatrix}.$$

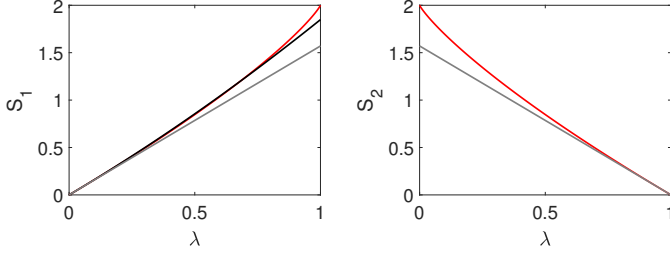


FIG. 7. Left: $S_1(\lambda)$ as a function of λ (red curve). The gray (black) curve shows the linear (quadratic) approximation of $S_1(\lambda)$ about $\lambda = -1$. Right: $S_2(\lambda)$ as a function of λ (red curve). The gray curve shows the linear approximation of $S_2(\lambda)$ about $\lambda = 1$.

Trace of the monodromy matrix for $0 < \lambda < 1$. We now finally ready to use the results of the previous section to compute the monodromy matrix for $0 < \lambda < 1$. In the sub-region $x \in (-\pi, c_1)$, we choose the fundamental matrix solution $Y(x)$ as in Eq. (24), with $v_+(x)$ and $v_-(x)$ given by Eq. (27). The value of this fundamental matrix solution at $x = -\pi$ is thus

$$Y(-\pi) = \begin{pmatrix} A_-(-\pi)e^{-S_2(\lambda)/2\epsilon} & A_+(-\pi)e^{S_2(\lambda)/2\epsilon} \\ \frac{1}{\epsilon}\sqrt{|Q(-\pi)|}A_-(-\pi)e^{-S_2(\lambda)/2\epsilon} & -\frac{1}{\epsilon}\sqrt{|Q(-\pi)|}A_+(-\pi)e^{S_2(\lambda)/2\epsilon} \end{pmatrix},$$

with A_{\pm} given by Eq. (28). Based on the above discussion, the value of the continuation of the above fundamental matrix solution at $x = \pi$ is given by

$$Y(\pi) = \begin{pmatrix} A_-(\pi)e^{S_2(\lambda)/2\epsilon} & A_+(\pi)e^{-S_2(\lambda)/2\epsilon} \\ \frac{1}{\epsilon}\sqrt{|Q(\pi)|}A_-(\pi)e^{S_2(\lambda)/2\epsilon} & -\frac{1}{\epsilon}\sqrt{|Q(\pi)|}A_+(\pi)e^{-S_2(\lambda)/2\epsilon} \end{pmatrix} C,$$

where C is the connection matrix given by

$$C = C_5 C_8 C_3 C_7 C_1 C_6 C_5 C_4 C_3 C_2 C_1. \quad (34)$$

Now recall that, as before, we can obtain the monodromy matrix via Eq. (25). Tedious but straightforward algebra then shows that the trace of the monodromy matrix is given by Eq. (7), with $S_1(\lambda)$ and $S_2(\lambda)$ given by Eq. (32) and Eq. (33), as before.

A.3 Calculation of relative bandwidth

Approximated expressions for $S_1(\lambda)$ and $S_2(\lambda)$. The functions $S_1(\lambda)$ and $S_2(\lambda)$ characterise the oscillating and the envelope part of the analytical expression of the trace of the monodromy matrix in Eq. (25). These are crucial quantities since $S_1(\lambda)$ determine the location of the bands through Eq. (9) and in turn the amplitudes and velocities of the relative soliton-like excitations, whereas the solitonic character of the band is fixed by the condition (11) which depends on $S_2(\lambda)$. In order to obtain explicit estimates of the number of

solitons along with their features (amplitudes and velocities) as a function of ϵ , it is worth to introduce appropriate Taylor expansions. Specifically, the Taylor expansions of $S_1(\lambda)$ around $\lambda = 0$ and of $S_2(\lambda)$ around $\lambda = 1$ are needed. Using known properties of elliptic integrals [63], one can verify that these expansions are given by the following expressions

$$S_1(\lambda) = \pi\lambda/2 + \sqrt{2}\pi\lambda^2/16 + O(\lambda^3), \quad (35a)$$

$$S_2(\lambda) = -\pi(\lambda - 1)/2 + O(\lambda - 1)^2, \quad (35b)$$

respectively.

Relative bandwidth. Here we give some details on the characterization of the bands. For $n \geq 1$, the width of the n -th spectral band, which is approximately centered at z_n , is given by $w_n = \lambda_{2n} - \lambda_{2n-1}$, while for $n = 0$, the bandwidth is given by $w_0 = \lambda_0$. The width of the n -th spectral gap is given by $g_n = \lambda_{2n+1} - \lambda_{2n}$. We first consider the Taylor expansion of $\text{tr}M$ around z_n (the location of the n -th maximum), evaluated at $\lambda = \lambda_{2n-1}$ and $\lambda = \lambda_{2n}$, and we obtain the n -th bandwidth as

$$w_n = \frac{2\epsilon}{|S'_1(z_n)|} \exp(-S_2(z_n)/\epsilon) + O(\epsilon e^{-2S_2(z_n)/\epsilon}).$$

Next we use the difference $z_{n+1} - z_n$ to approximate $w_n + g_n$. To do so, we first show the difference between these two quantities is given by

$$(w_n + g_n) - (z_{n+1} - z_n) = O(\epsilon e^{-S_2(z_{n+1})/\epsilon}).$$

We then expand $S_1(\lambda)$ around z_n , evaluate at $\lambda = z_{n+1}$ and obtain

$$z_{n+1} - z_n = \pi\epsilon/S'_1(z_n) + O(\epsilon^2).$$

Combining all the above results, we finally obtain the asymptotic expression for the n -th relative bandwidth in Eq. (10).

-
- [1] E. Fermi, J. Pasta and S. Ulam, *Studies of nonlinear problems*, in *Collected Papers of Enrico Fermi*, E. Segré, Ed. (University of Chicago, Chicago, 1965), Vol. 2.
 - [2] J.L. Tuck and M.T. Menzel, *Adv. Math.* **9**, 399 (1972).
 - [3] J. Ford, *Phys. Rep.* **213**, 271-310 (1992).
 - [4] G. P. Berman and F. M. Izrailev, *Chaos* **15**, 015104 (2005).
 - [5] T. Dauxois, M. Peyrard and S. Ruffo, *Eur. J. Phys.* **26**, S3 (2005).
 - [6] G. Gallavotti (ed.) *The Fermi-Pasta-Ulam problem: a status report*, Lect. Note Phys. **728** (Springer, Berlin-Heidelberg, 2008).
 - [7] M. A. Porter, N. J. Zabusky, B. Hu and D. K. Campbell, *Am. Sci.* **97**, 214 (2009).
 - [8] G. Benettin, H. Christodoulidi, A. Poino, *J. Stat. Phys.* **152**, 195 (2013).
 - [9] M. Onorato, L. Vozella, D. Proment, and Y. V. Lvov, *PNAS* **112**, 4208 (2015).
 - [10] C. Bao, J. A. Jaramillo-Villegas, Y. Xuan, D. E. Leaird, M. Qi, and A. M. Weiner, *Phys. Rev. Lett.* **117**, 163901 (2016).
 - [11] M. Guasoni, J. Garnier, B. Rumpf, D. Sugny, J. Fatome, F. Amrani, G. Millot, and A. Picozzi, *Phys. Rev. X* **7**, 011025 (2017).

- [12] N. Zabusky and M. Kruskal, *Phys. Rev. Lett.* **15**, 240–243 (1965).
- [13] J. Korteweg and G. De Vries, *Phil. Mag.* **39**, 422 (1895).
- [14] P. Lorenzoni and S. Paleari, *Physica D* **221**, 110 (2006).
- [15] M. Toda, *J. Phys. Soc. Jpn.* **26**, 235 (1969).
- [16] M. Toda, *Theory of nonlinear lattices* (Springer, New York, 1981).
- [17] R. Hirota and K. Suzuki, *J. Phys. Soc. Jpn.* **28**, 1366 (1970).
- [18] H. Ikezi, *Phys. Fluids* **16**, 1668 (1973).
- [19] S. Trillo, G. Deng, G. Biondini, M. Klein, G. F. Clauss, A. Chabchoub and M. Onorato, *Phys. Rev. Lett.* **117**, 144102 (2016).
- [20] Y. C. Mo, R. A. Kiskheh, D. Feldman, I. Haber, B. Beaudoin, P. G. O’Shea, and J. C. T. Thangaraj, *Phys. Rev. Lett.* **110**, 084802 (2013).
- [21] W. E. Ferguson, H. Flaschka, and D. W. McLaughlin, *J. Comp. Phys.* **45**, 157 (1982).
- [22] N.M. Ercolani, I. R. Gabbitov, C. D. Levermore, and D. Serre, eds., *Singular Limits of Dispersive Waves*, NATO ASI Series, Ser. B 320 (Plenum Press, New York, 1994).
- [23] G. A. El and M. A. Hoefer, *Physica D* **333**, 11 (2016).
- [24] Z. Dutton, M. Budde, C. Slowe, L. V. Hau, *Science* **293**, 663 (2001).
- [25] M. A. Hoefer, M. J. Ablowitz, I. Coddington, E. A. Cornell, P. Engels, and V. Schweikhard, *Phys. Rev. A* **74**, 023623 (2006).
- [26] W. Wan, S. Jia, and J. W. Fleischer, *Nature Phys.* **3**, 46 (2007).
- [27] N. Ghofraniha, C. Conti, G. Ruocco, and S. Trillo, *Phys. Rev. Lett.* **99**, 043903 (2007).
- [28] C. Conti, A. Fratolocchi, M. Peccianti, G. Ruocco, and S. Trillo, *Phys. Rev. Lett.* **102**, 083902 (2009).
- [29] S. Trillo and A. Valiani, *Opt. Lett.* **35**, 3967 (2010).
- [30] J. Fatome, C. Finot, G. Millot, A. Armaroli and S. Trillo, *Phys. Rev. X* **4**, 021022 (2014).
- [31] A. Moro and S. Trillo, *Phys. Rev. E* **89**, 023202 (2014).
- [32] G. Xu, M. Conforti, A. Kudlinski, A. Mussot, and S. Trillo, *Phys. Rev. Lett.* **118**, 254101 (2017).
- [33] P. A. P. Janantha, P. Sprenger, M. A. Hoefer, and M. Wu, *Phys. Rev. Lett.* **119**, 024101 (2017).
- [34] P. D. Miller and Z. Xu, *Commun. Pure Appl. Math.* **64**, 205 (2010).
- [35] J. Garnier, G. Xu, S. Trillo, and A. Picozzi, *Phys. Rev. Lett.* **111**, 113902 (2013).
- [36] B. L. Holian, H. Flaschka and D. W. McLaughlin, *Phys. Rev. A* **24**, 2595 (1981).
- [37] S. Venakides, P. Deift, and R. Oba, *Commun. Pure Applied Math.* **44**, 1171 (1991).
- [38] R. F. Bibkaev, *J. Math. Sciences* **77**, 3033 (1995).
- [39] B. M. Lake, H. C. Yuen, H. Rungaldier and W. E. Ferguson, *J. Fluid Mech.* **83**, 49 (1977).
- [40] H. C. Yuen and W. E. Ferguson, *Phys. Fluids* **21**, 1275 (1978).
- [41] N. N. Akhmediev, V.M. Eleonosskii, and N.E. Kulagin, *Sov. Phys. JETP* **62**, 894 (1985).
- [42] S. Trillo and S. Wabnitz, *Opt. Lett.* **16**, 986 (1991).
- [43] G. Van Simaey, Ph. Emplit, and M. Haelterman, *Phys. Rev. Lett.* **87**, 033902 (2001).
- [44] O. Kimmoun, H.C. Hsu, H. Branger, M.S. Li, Y.Y. Chen, C. Kharif, M. Onorato, E. J. R. Kelleher, B. Kibler, N. Akhmediev, and A. Chabchoub, *Sci. Rep.* **6**, 28516 (2016).
- [45] B. Dubrovin, T. Grava, and C. Klein, *J. Nonlinear Sci.* **19**, 57 (2009).
- [46] P. D. Miller and S. Kamvissis, *Phys. Lett. A* **247**, 75 (1998).
- [47] S. Kamvissis, K. T. R. McLaughlin, and P. D. Miller, *Semiclassical soliton ensembles for the focusing nonlinear Schrödinger equation*, (Princeton University Press, Princeton, 2003).
- [48] M. J. Ablowitz and H. Segur, *Solitons and the inverse scattering transform* (SIAM, Philadelphia, 1981)
- [49] E. Infeld and G. Rowlands, *Nonlinear waves, solitons and chaos* (Cambridge University Press, Cambridge, 2000)
- [50] G. P. Agrawal, *Nonlinear fiber optics* (Academic Press, New York, 2007)
- [51] J. R. Thompson and R. Roy, *Phys. Rev. A* **43**, 4987 (1991).
- [52] S. Trillo, S. Wabnitz, and T. A. B. Kennedy, *Phys. Rev. A* **50**, 1732 (1994).
- [53] A.R. Its and V.P. Kotlyarov, *Dokl. Akad. Nauk Ukr. RSR A* **11**, 965 (1976).
- [54] Y. Ma and M. Ablowitz, *Stud. Appl. Math.* **65**, 113 (1981).
- [55] E.D. Belokolos, A.I. Bobenko, V.Z. Enol’skii and A.R. Its, *Algebro-geometric approach to nonlinear integrable equations* (Springer, New York, 1994).
- [56] C. S. West and T. A. B. Kennedy, *Phys. Rev. A* **47**, 1252 (1993).
- [57] A. Messiah, *Quantum mechanics, Vol. I* (Elsevier, Amsterdam, 1961)
- [58] G. Deng, G. Biondini and S. Trillo, *Physica D* **333**, 137 (2016).
- [59] A.R. Osborne and L. Bergamasco, *Physica D* **18**, 26 (1986).
- [60] A. Fratolocchi, C. Conti, G. Ruocco, and S. Trillo, *Phys. Rev. Lett.* **101**, 044101 (2008).
- [61] P. V. Mamyshev, P. G. Wigley, J. Wilson, C. Bosshard, and G.I. Stegeman, *Appl. Phys. Lett.* **64**, 3374 (1994)
- [62] P. V. Mamyshev, C. Bosshard, and G.I. Stegeman, *J. Opt. Soc. Am. B.* **11**, 1254 (1994).
- [63] F. W. Olver, D. W. Lozier, R. F. Boisvert and C. W. Clark, *NIST Handbook of Mathematical Functions*, (Cambridge University Press, New York, 2010)